Supplementary Figures

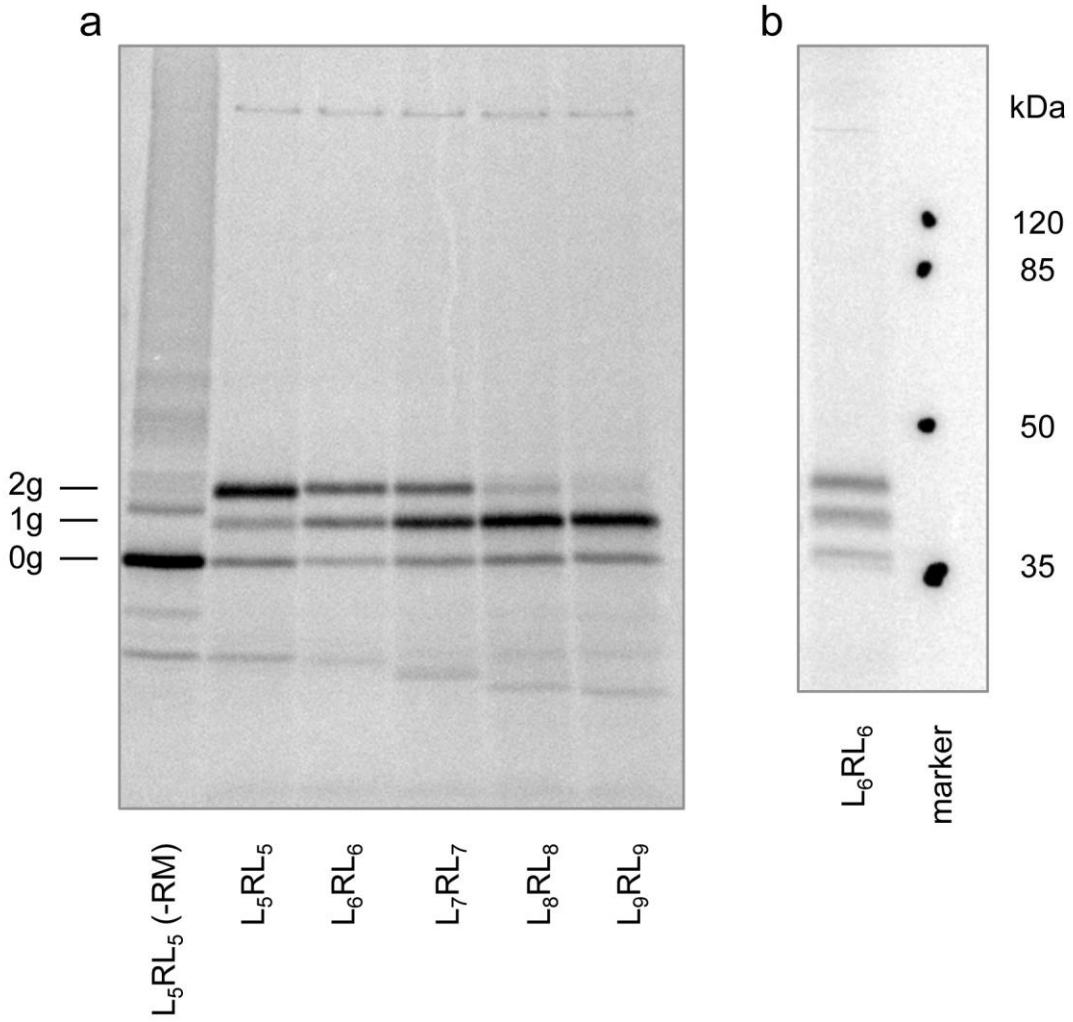

Supplementary Figure 1. (a) Uncropped version of Fig. 2a. –RM indicates that the translation was done in the absence of rough mcirosomes. (b) LepB construct containing the GGPG-L6RL6-GPGG H-segment, with Mw marker. The theoretical Mw of the LepB construct is 34.9 kDa.

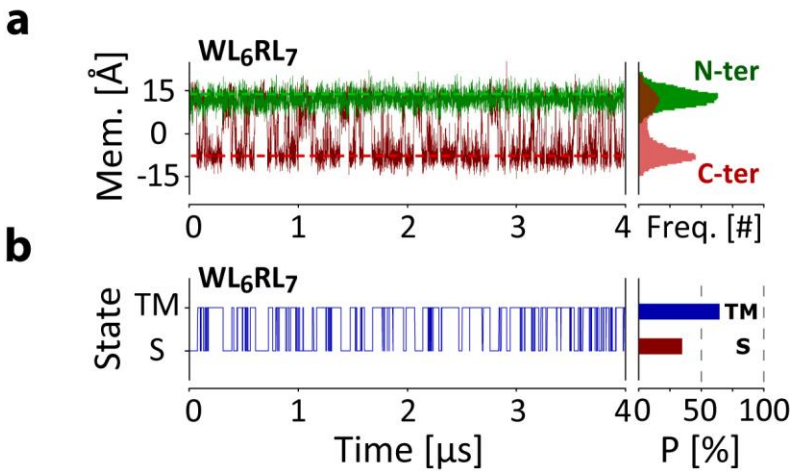

Supplementary Figure 2. Control simulation of GWL_6RL_7G. The simulation shows that the N-terminal Leu→Trp substitution, which facilitates purification and concentration determination in the synthetic implementation, does not alter the partitioning properties and insertion propensity of the peptide. **a.** Even though only the C-terminus partitions for this peptide, presumably due to Trp-anchoring of the N-terminus, the partitioning properties determined from the motion of the peptide termini are very similar. **b.** Quantification of the insertion propensity gives a value of P_{TM} = 64.2±5.3 for GWL_6RL_7G, which is within the error of the P_{TM} = 65.8±9.1 for the GL_7RL_7G peptide (see Figure 3 and Table 1).

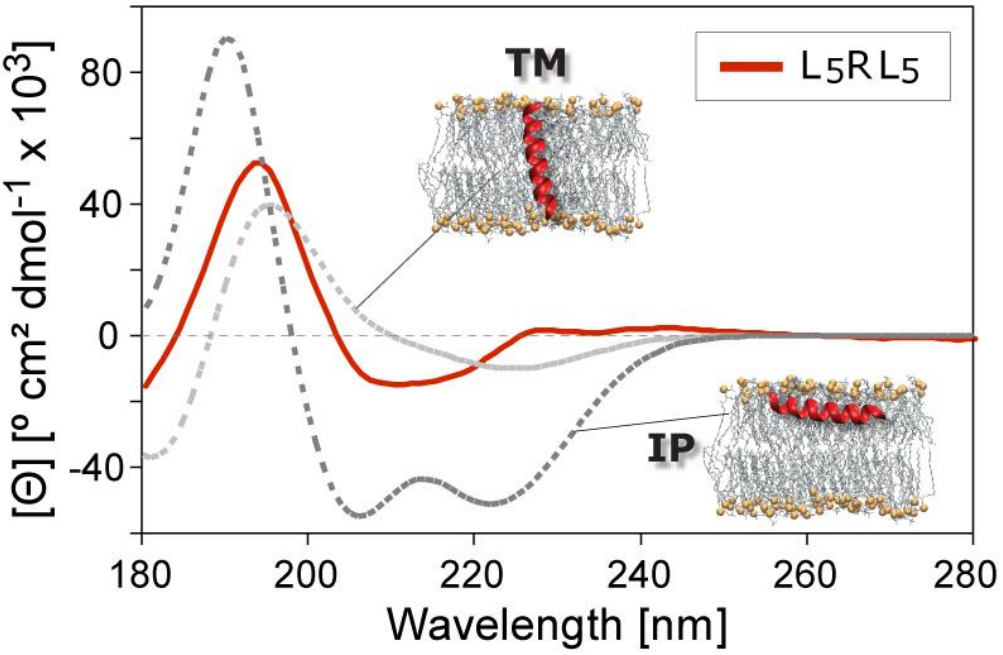

Supplementary Figure 3. L_5RL_5 Oriented SRCD spectrum. The spectrum (red) exhibits an exciton peak centered at ~229 nm, unlike the other peptides; this may be indicative of tryptophan-tryptophan interactions, which in turn suggests that the peptide aggregates. This precludes a clear deconvolution[3,4] of the in-plane (IP) and transmembrane (TM) contributions for this peptide.

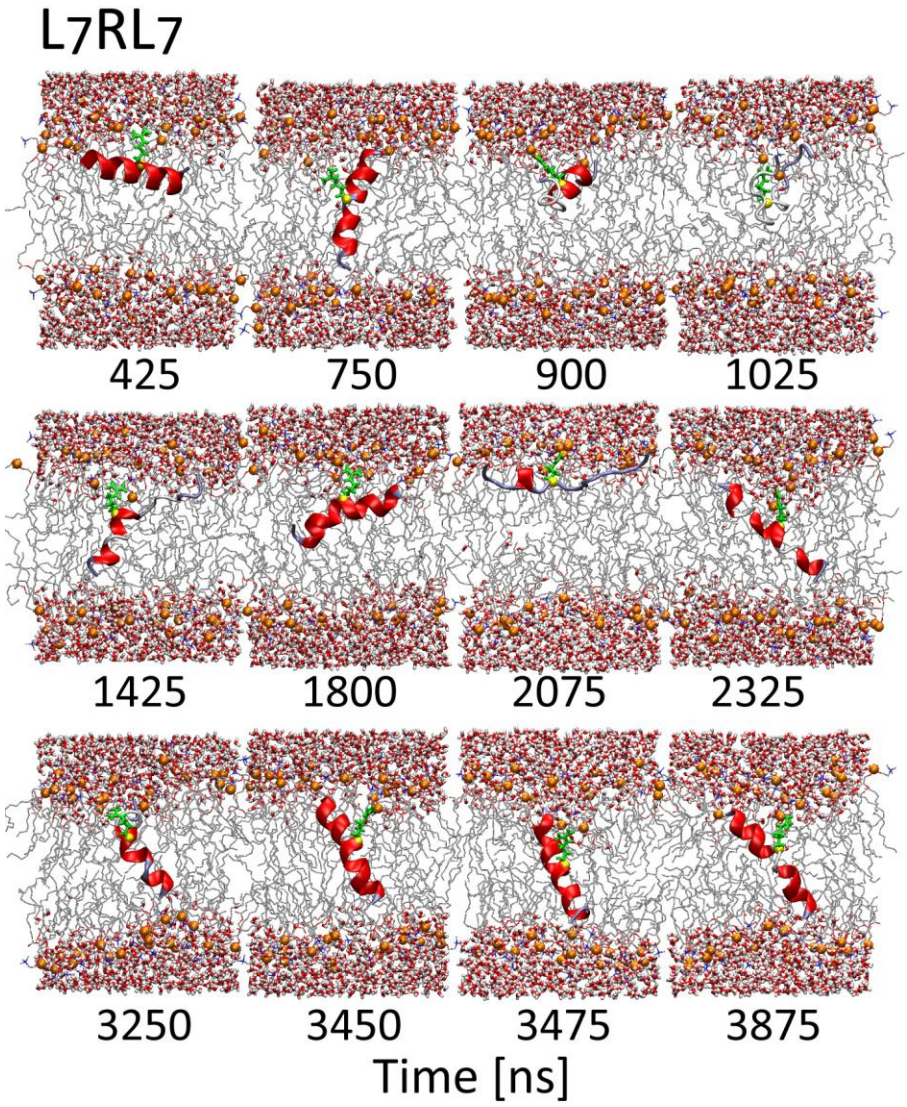

Supplementary Figure 4. Configurational ensemble. The figure illustrates the broad range of conformations sampled in the membrane by all peptides (show here is the OPLS simulation of the L_7RL_7 peptide). The figure is only indicative and does not represent a comprehensive conformational analysis. Some states shown here are extremely rare (e.g. the unfolded peptide in 1025 ns occurs only once), while others, such as the interfacial and TM helices (450 & 750 ns), are abundant. Partially folded helices are found frequently at the interface (2075 ns), and occasionally span the bilayer (1425 ns) or insert partially (900 ns). Some configurations represent intermediates of peptides about to translocate a terminus (1800 ns). Strongly tilted TM helices are abundant and stable, typically resulting in noticeable bilayer distortions on one (2325 & 3475 ns), or both lipid leaflets (3250 & 3875 ns). The L_7RL_7 simulation with the CHARMM force field shows no unfolded states at equilibrium, but the resulting free energies are similar. At present it is not clear which force field is more realistic.

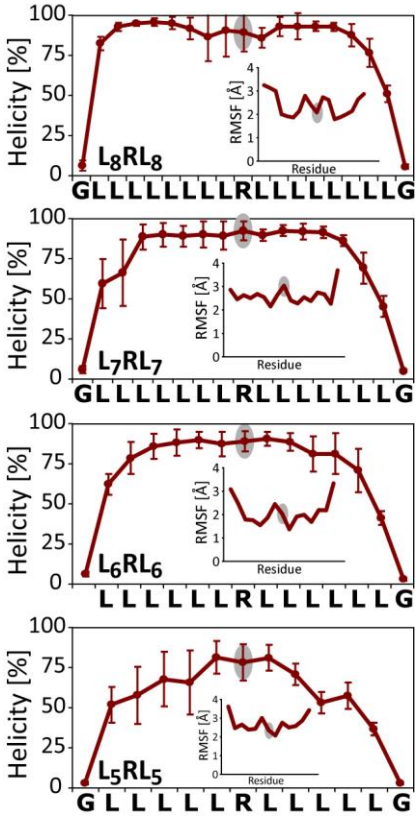

Supplementary Figure 5. Peptide helicity and structural flexibility. The panels show the peptide helicity and α-carbon root mean square fluctuation (RMSF), averaged over the equilibrium phase of the simulations. All peptides display high helicity and the central arginine residue (highlighted) is generally inconspicuous. The lower helicity of the shortest peptide (L_5RL_5) is due to its predominantly interfacial location, which has a lower energetic penalty for unfolded conformers.

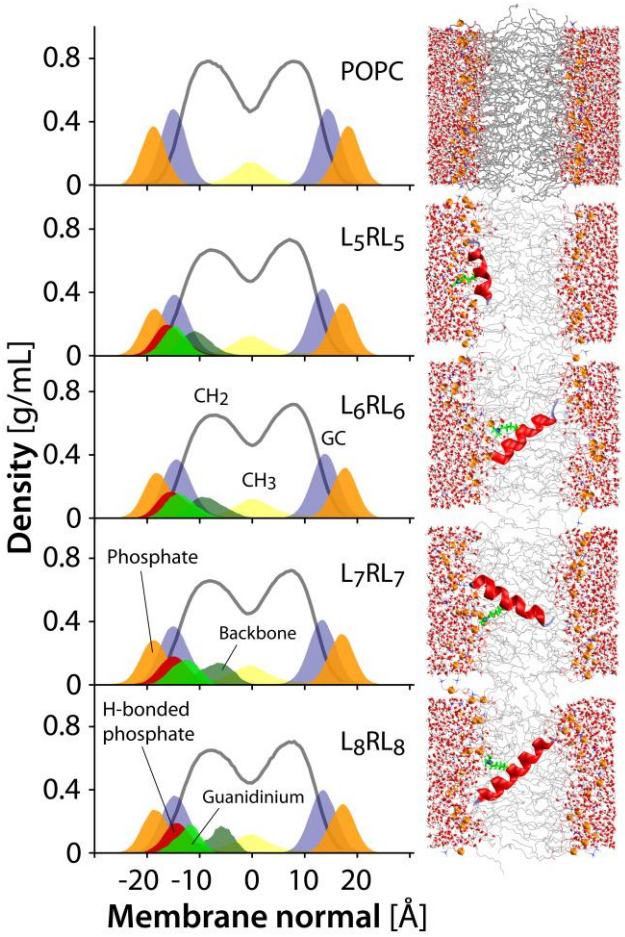

Supplementary Figure 6. Transbilayer density profiles. The trans-bilayer density profiles of arginine together with the principal structural groups of the lipid bilayer (GC = glycerol carbonyls), show the bilayer response to charge burial. The profiles are time-averaged over the equilibrium part of the simulation. The figure shows the distributions of the charged guanidinium moiety (light green) and backbone (dark green) of arginine together with the distribution of the phosphates hydrogen-bonded to arginine. Deeper burial of the guanidinium group results in hydrogen-bonded phosphate groups (red) being 'pulled' into the hydrophobic part of the membrane. The guanidinium group remains tightly hydrogen-bonded to lipid phosphate headgroups throughout the simulations for all peptides (see Table S1).

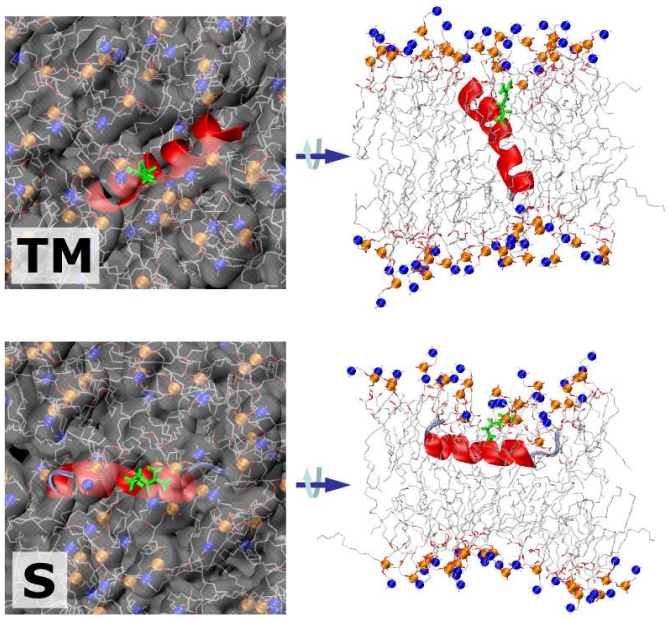

Supplementary Figure 7. Burial of the guanidinium group. Local bilayer deformations, caused by guanidinium-phosphate hydrogen bonds (see Table TS1) that 'pull down' lipid headgroups into the hydrophobic membrane core (see Figure S3), enable arginine to retains direct access to water for both the TM and S configurations.

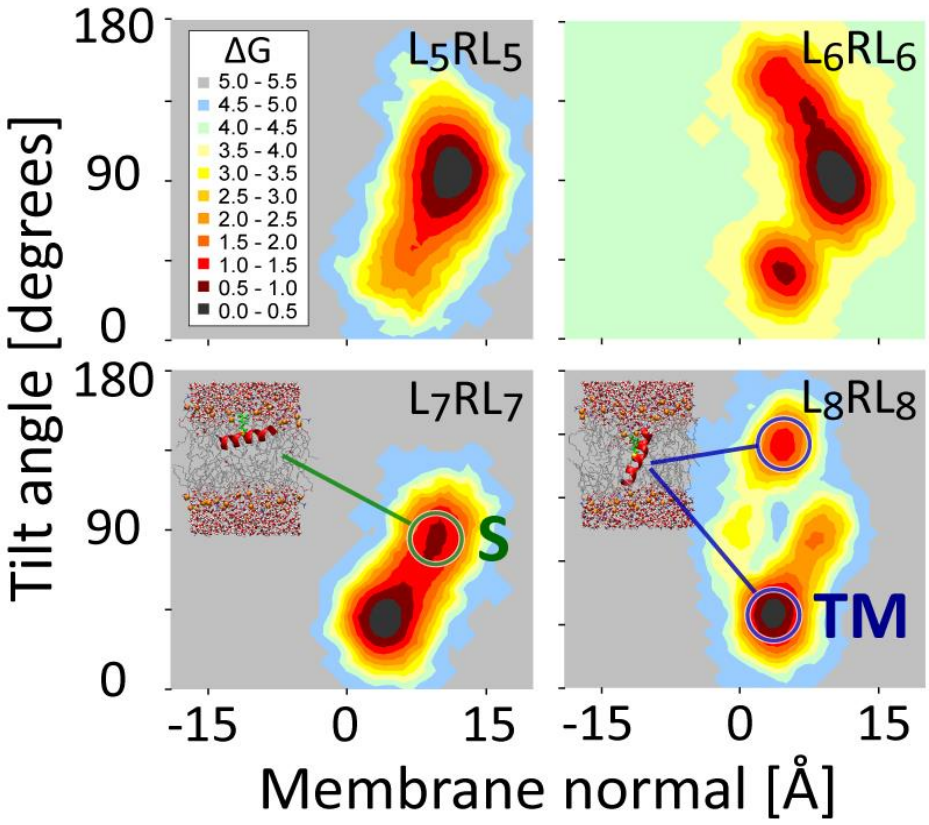

Supplementary Figure 8. Peptide partitioning free energy surface. The two dimensional free energy surface is constructed from the distribution of the helix tilt angle versus the peptide center of mass of the equilibrium part of the simulations. All peptides show both interfacial (S) and transmembrane (TM) minima. The surface reveals that $L_{10}R_6$ is predominantly at the interface (S state: z ≈ 11 Å, tilt ≈ 90°). L_6RL_6 and L_7RL_7 have significant populations of both S and TM states, while $L_{16}R_9$ is predominantly inserted (TM state: z ≈ 3 Å, tilt ≈ 20°). L_6RL_6 and L_8RL_8 show insertion from both termini (z ≈ 3 Å, tilt ≈ 20° and tilt ≈ 160°).

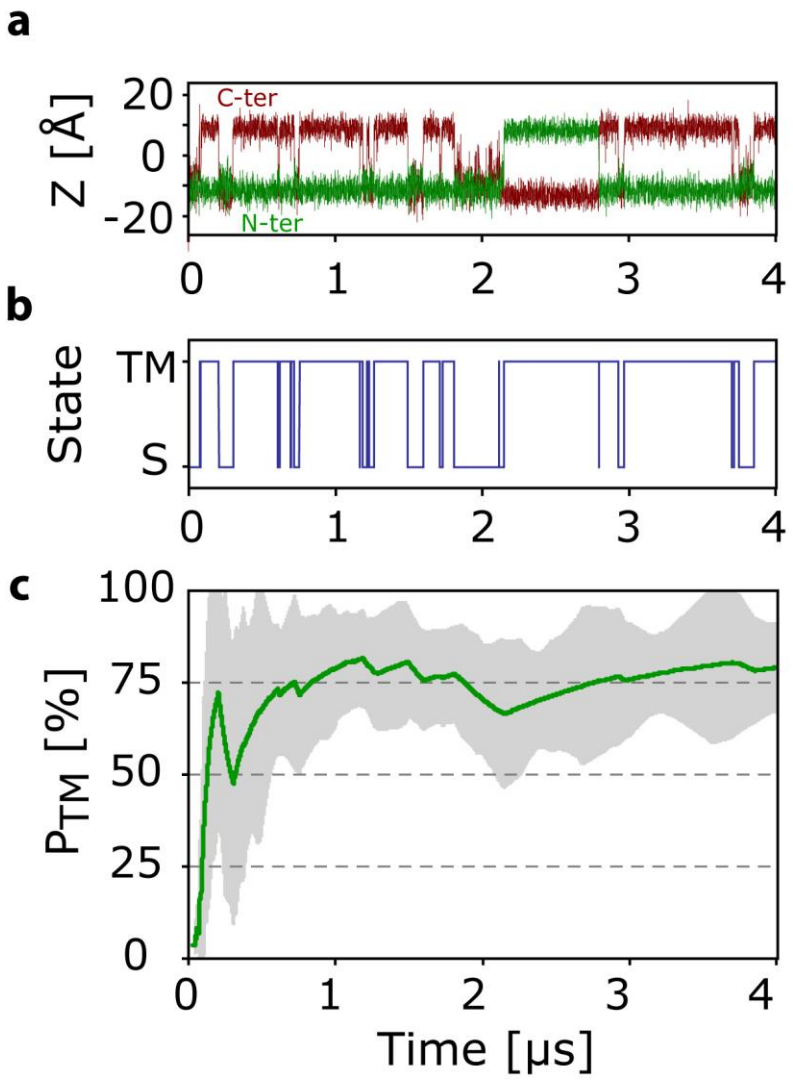

Supplementary Figure 9. Control simulation of the L_7RL_7 peptide with the CHARMM27/36 force field. The thermodynamic results are very similar (see Table 1). **a:** The increased helicity of the CHARMM force field leads to 'cleaner' transitions, which can be visualized by plotting the positions of the peptide termini along the membrane normal. **b:** The positions of the termini allow determination of the transmembrane and surface bound state kinetics, which are ~3.3x slower for the CHARMM simulation. **c:** The reduced transition rate requires longer simulations for proper convergence.

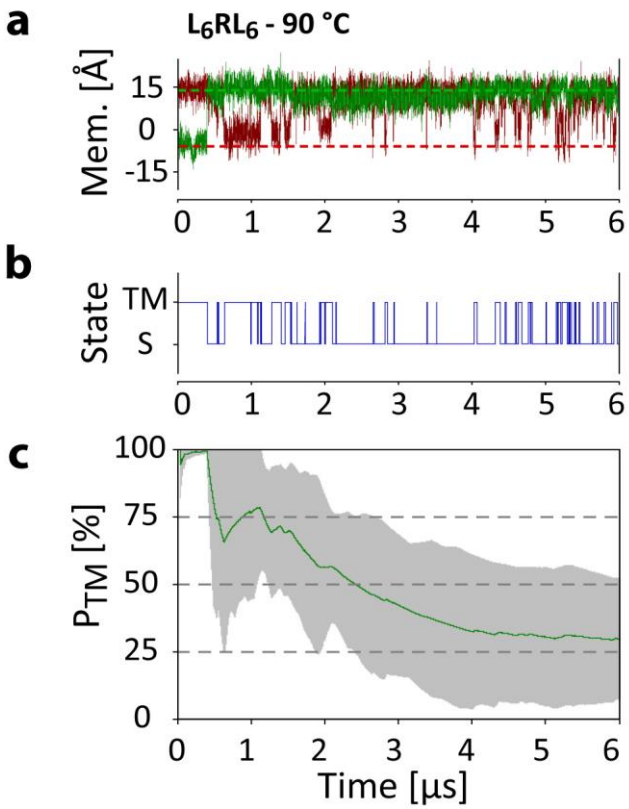

Supplementary Figure 10. Control simulation of L_6RL_6 at 90 °C. a. The simulation shows decreased partitioning kinetics compared to the 140 °C simulations (see Figure 3). **b.** While the overall insertion propensity P_{TM} = 29.9±24.4 % at 90 °C is similar to P_{TM} = 35.3±7.6 % at 140 °C, the reduction in temperature results in a reduced rate of transitions. **c.** The convergence graph shows that 6 µs are insufficient for accurate determination of the equilibrium insertion ratio.

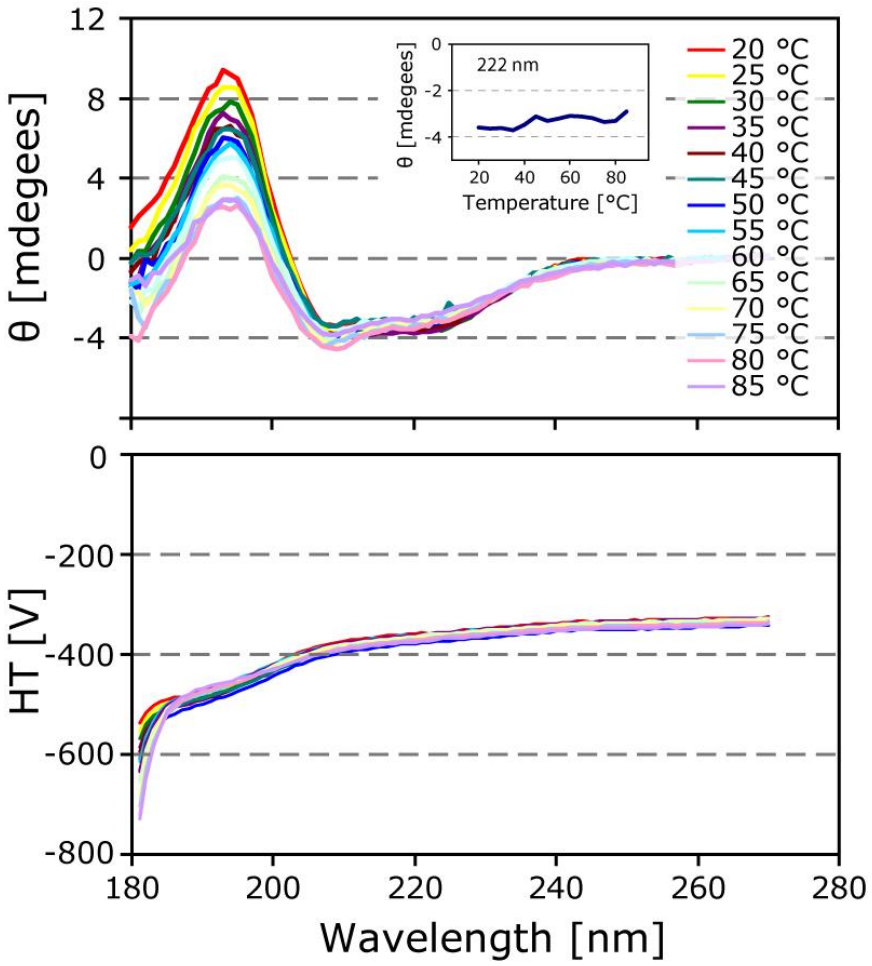

Supplementary Figure 11. Experimental thermostability of L_7RL_7. The peptide was incorporated into POPC LUVs and SRCD spectra were recorded as a function of temperature in the range 20 to 85 ºC. The CD spectra (upper panel) have three distinctive extrema at 208, 222, and 193 nm, which are characteristic of an isotropic distribution of α-helices in the beam, as expected for hydrophobic peptides embedded in the lipid bilayers. While the 193 nm peak diminishes at higher temperatures (possibly due to vesicle aggregation), the ellipticity at 222 nm, which is directly proportional to the peptide helicity does not show significant change (inset), and no unfolding transition is observed over this entire temperature range. The ellipticity at 222 nm, which is directly proportional to the peptide helicity, does not show significant change (inset), suggesting no unfolding transition is observed over this entire temperature range. While the 193 nm peak diminishes at higher temperatures (possibly due to non-specific peptide-peptide interactions, there are no exciton peaks indicative of specific peptide-peptide interactions as were seen in the oriented specimens, and the corresponding HT curves (lower panel) are all essentially identical, ruling out LUV aggregation during the heating process.

Supplementary Tables

Supplementary Table 1. Lipid phosphate-guanidinium hydrogen-bonding. The table shows the average number of hydrogen bonds between the guanidinium group and the lipid phosphates. The second column shows fraction of the simulation for which at least one hydrogen bond between arginine and a phosphate is present. The numbers are nearly identical for all simulations.

Peptide	PO_4 – guanidinium contacts [#]	Hydrogen-bonded [%]
L_5RL_5	2.1 ± 0.7	98.2
L_6RL_6	1.9 ± 0.7	96.6
L_7RL_7	1.9 ± 0.6	97.4
L_8RL_8	2.0 ± 0.7	96.6

Supplementary Table 2. Transfer free energy as a function of the number of leucine residues. The whole peptide transfer free energy ΔG(*n*) for pure polyleucine (L_n) peptides, and polyleucine peptides containing a single central arginine residue ($L_{n/2}RL_{n/2}$), varies linearly with the total number of leucine residues in the peptide *n*. The table shows the best fits of the simulation and experimental translocon data to equation ES1 above, where ΔG(*n*) is the whole peptide transfer free energy, M is the slope, *n* the total number of leucine residues, and ΔG_0 the offset (insertion free energy at zero leucines). The general agreement of the slopes is remarkable, while the difference between simulation and experiments stems virtually entirely due to a 2 kcal/mol offset for pure polyleucine peptides. Peptide sequences are (1) L_n with n = 5,6,7,8,9,10,12; and (2) $GL_{n/2}RL_{n/2}G$ with n = 10,12,14,16.

$$\Delta G(n) = M \cdot n + \Delta G_0, \quad n = \text{total number of leucine residues} \qquad \text{(ES3)}$$

System	M [kcal/mol/Leu]	ΔG_0 [kcal/mol]	X^2
L_n (exp.)	-0.8	7.7	0.3
L_n (sim.)	-0.8	5.7	0.1
$L_{n/2}RL_{n/2}$ (exp.)	-0.5	6.3	0.2
$L_{n/2}RL_{n/2}$ (sim.)	-0.6	7.8	0.2
ΔΔG (exp.)	0.3	-0.6	-
ΔΔG (sim.)	0.2	2.9	-

Supplementary References

1 Ulmschneider, M. B., Doux, J. P. F., Killian, J. A., Smith, J. & Ulmschneider, J. P. Mechanism and kinetics of peptide partitioning into membranes. *J. Am. Chem. Soc.* **132**, 3452-3460 (2010).

2 Ulmschneider, J. P., Smith, J. C., White, S. H. & Ulmschneider, M. B. In silico partitioning and transmembrane insertion of hydrophobic peptides under equilibrium conditions. *J. Am. Chem. Soc.* **133**, 15487-15495 (2011).

3 Vogel, H. Comparison of the conformation and orientation of alamethicin and melittin in lipid membranes. *Biochemistry* **26**, 4562-4572 (1987).

4 Wu, Y., Huang, H. W. & Olah, G. A. Method of oriented circular dichroism. *Biophys. J.* **57**, 797-806 (1990).